Applied Catalysis A: General 522 (2016) 130–137

Contents lists available at ScienceDirect

Applied Catalysis A: General

journal homepage: www.elsevier.com/locate/apcata

Total oxidation of ethanol over $Au/Ce_{0.5}Zr_{0.5}O_2$ cordierite monolithic catalysts

Pavel Topka [a,*], Mariana Klementová [b]

[a] Institute of Chemical Process Fundamentals of the Czech Academy of Sciences, v. v. i., Rozvojová 2/135, 165 02 Praha 6, Czech Republic
[b] University of West Bohemia, New Technologies – Research Centre, 306 14 Plzeň, Czech Republic

ARTICLE INFO

Article history:
Received 15 December 2015
Received in revised form 2 May 2016
Accepted 3 May 2016
Available online 4 May 2016

Keywords:
Oxidation
Volatile organic compounds
Gold
Ceria-zirconia mixed oxide
Ethanol
Monoliths

ABSTRACT

The aim of this work was to propose the methods for gold introduction during the preparation of monolithic catalysts and to investigate their effect on catalyst properties. Two types of catalysts were prepared: (i) monoliths washcoated with gold/ceria-zirconia powder, and (ii) gold deposited on the monoliths washcoated with ceria-zirconia powder. An important part of the work was the characterization of the catalysts, in particular Au particle size and redox properties. Catalytic performance and selectivity were evaluated using ethanol gas-phase oxidation. It was shown that the enhanced reducibility of the catalysts with higher Au dispersion leads to improved catalytic performance.

1. Introduction

Volatile organic compounds (VOC) are known as one of the major contributors to air pollution. They may have short and long-term adverse health effects, act as greenhouse gases and control the rate of oxidant formation during the production of ground-level ozone, which is the primary constituent of the photochemical smog [1,2]. Catalytic oxidation is regarded as an efficient, cost-effective and environmentally friendly way to treat VOC emissions [3]. It is due to the fact that the use of catalysts leads to lower reaction temperatures and avoids the generation of dangerous reaction by-products like NOx [4].

The most commonly used VOC oxidation catalysts are based on supported noble metals or transition metal oxides. Metal oxides, mainly of Co, Cu, Ni and Mn, have the advantage of having lower cost and greater resistance to deactivation by poisoning [5]. However, noble metal catalysts are generally preferred because of their high activity, excellent stability and good selectivity to CO_2 [6].

Since the pioneering work by Haruta et al. [7], gold catalysts supported on different metal oxides have been reported to be efficient catalysts for oxidation reactions. The importance of the nature of the support for the catalytic activity of gold catalysts was underlined by Scirè and Liotta [8]. The support could not only affect the amount of gold anchored on the surface, the size and the shape of gold particles, but also participate in the reaction pathway when reducible oxides are used. Ceria is a very suitable support because of its ability to maintain a high gold dispersion and to take part in the oxidation reaction providing active oxygen species via Mars-van Krevelen mechanism [9]. The high activity of gold/ceria catalysts towards oxidation reactions has been attributed to the enhanced reactivity of CeO_2 surface oxygens induced by the metal, which causes a decrease in the strength of the surface Ce-O bonds adjacent to the active metal atoms thus leading to a higher surface lattice oxygen mobility of ceria [10]. The oxidation activity has been found to depend on both the capacity of the oxide to provide active lattice oxygens and the oxygen activation on the active metal [11].

More recently, ceria-zirconia mixed oxides were proposed as supports for the VOC oxidation catalysts [12,13]. It was demonstrated that the partial substitution of cerium with zirconium leads to improved redox properties, higher oxygen storage capacity and increased catalytic activity at low temperatures [14]. We have shown that depending on the type of VOC, the introduction of gold can increase catalytic performance and/or selectivity of ceria-zirconia catalysts in the oxidation of chlorobenzene, dichloromethane, ethanol and toluene [15–17].

These previous studies were carried out using powder catalysts. Nevertheless, the implementation of catalysts in industry requires the use of suitable supports, such as ceramic or metallic honey-

* Corresponding author.
E-mail address: topka@icpf.cas.cz (P. Topka).

http://dx.doi.org/10.1016/j.apcata.2016.05.004
0926-860X/

comb monoliths, due to high pressure drop of powder catalysts at high flow rates. Martínez Tejada et al. [18] recently demonstrated that ceria-based gold catalysts can be successfully deposited on ferritic stainless steel and aluminium monoliths. However, ceramic cordierite monoliths are often preferred over metallic due to high mechanical stability and low thermal expansion coefficient, which resulted in their successful application in automotive catalytic converters and in industry. To the best of our knowledge, ceria or ceria-zirconia supported gold catalysts washcoated on cordierite monoliths have not yet been studied.

The aim of this work was to investigate the preparation of cordierite monolithic catalysts with gold supported on ceria-zirconia as an active phase. The $Au/Ce_{0.5}Zr_{0.5}O_2$ catalysts were prepared via direct anionic exchange method, which appears to be particularly interesting as it leads to highly active oxidation catalysts. Washcoating with ready-made gold/ceria-zirconia catalysts and deposition of gold onto ceria-zirconia washcoat were compared and the catalytic performance in ethanol total oxidation was correlated with physicochemical properties of the catalysts.

2. Experimental

2.1. Catalyst preparation

The cylindrical cordierite monoliths of diameter 26 mm, length 20 mm, and average weight 6.32 g, with 200 cpsi and square channels (Céramiques Techniques Industrielles, France) were calcined in a batch furnace in static air at 500 °C for 4 h before further treatments.

The washcoated monoliths were prepared by manually controlled dipping of a monolith in a slurry composed of diluted nitric acid solution (1.4 wt.%) and 15 wt.% of ceria-zirconia mixed oxide ($Ce_{0.5}Zr_{0.5}O_2$, < 50 nm particle size (BET), Aldrich) [19]. Typically, several dips were needed to obtain the desired amount of washcoat loading. In each cycle the excess slurry was removed by blowing air through the channels and then the samples were dried at 120 °C and calcined in air at 300 °C for 4 h. The monoliths washcoated with ceria-zirconia mixed oxide were labelled as CeZr.

Powder gold catalyst was prepared by the direct anionic exchange method of gold species with hydroxyl groups of the support [20]. 2.25×10^{-4} M aqueous solution of $HAuCl_4$ was heated up to 70 °C and the ceria-zirconia support was introduced in the amount corresponding to nominal Au loading 2 wt.%. After 1 h of thermostating and vigorous stirring, the suspension was centrifuged and the catalyst was washed with 4 M ammonia solution at 25 °C for 1 h. After drying in an oven at 120 °C overnight, the catalyst was calcined in air at 300 °C for 4 h. Finally, the prepared powder catalyst was washcoated on the cordierite monolith as described above. The monoliths washcoated with gold powder catalyst were labelled as AuCeZr.

Alternatively, gold was deposited on the monolith already washcoated with ceria-zirconia mixed oxide, which was prepared using the above-described procedure. 2.25×10^{-4} M aqueous solution of $HAuCl_4$ was heated up to 70 °C and a monolith with ceria-zirconia washcoat was introduced. The nominal Au loading was 2 wt.%. After 1 h of thermostating and vigorous stirring, the prepared catalyst was removed and washed with 4 M ammonia solution at 25 °C for 1 h. After drying in an oven at 120 °C overnight, the catalyst was calcined in air at 300 °C for 4 h. These catalysts were labelled as Au/CeZr.

2.2. Characterization

The catalysts were characterized by atomic emission spectroscopy with inductively coupled plasma atomic (ICP-AES), X-ray powder diffraction (XRD), transmission electron microscopy (TEM), X-ray photoelectron spectroscopy (XPS), N_2 physisorption, temperature programmed reduction by hydrogen (H_2-TPR), and temperature programmed desorption (TPD) of NH_3 and CO_2.

Chemical analysis of catalysts was done in ALS Czech Republic using an ICP-AES analyzer.

Powder X-ray diffraction data were obtained using a Bruker D8 Discover powder diffractometer equipped with a LynxEye detector and a primary double-crystal Si monochromator providing $CuK\alpha_1$ radiation. The data were refined using the TOPAS software. LaB6 (NIST standard reference material #660) was employed as a reference material for modelling the instrumental broadening.

Transmission electron microscopy (TEM) and scanning TEM (STEM) was carried out on a JEOL JEM 2200FS microscope operating at 200 kV (autoemission Shotky gun, point resolution 0.19 nm) with an in-column energy filter, a HAADF detector, and an EDX silicon drift detector Oxford Instruments X-Max attached. Images were recorded on a Gatan CCD camera with resolution 2048 × 2048 pixels using the Digital Micrograph software package. EDX analyses were acquired and treated in the INCA software package. Powder samples were dispersed in ethanol and the suspension was treated in ultrasound for 5 min. A drop of very dilute suspension was placed on a holey-carbon-coated copper grid and allowed to dry by evaporation at ambient temperature.

XPS spectra were recorded on a Kratos ESCA 3400 photoelectron spectrometer equipped with a polychromatic Mg X-Ray source (Mg Kα, 1253.4 eV) under the pressure of 5×10^{-7} Pa. Before the measurement, the samples were sputtered with Ar^+ ions at 500 V with 10 mA current for 30 s to remove superficial layers. All binding energies were calculated taking as reference the C–(C,H) component of the C 1s peak fixed at 284.8 eV. The overlapping spectral features were resolved into individual components using the damped non-linear least squares method and the lines of Gaussian-Lorentzian shape. Prior to fitting the Shirley background was subtracted.

N_2 physisorption on catalysts was performed using Micromeritics ASAP 2020 instrument after drying at 105 °C under 1 Pa vacuum for 24 h. The adsorption-desorption isotherms of nitrogen at −196 °C were treated by the standard Brunauer–Emmett–Teller (BET) procedure to calculate the specific surface area S_{BET}. The surface area of mesopores S_{meso} and the volume of micropores V_{micro} were determined by t-plot method using Lecloux-Pirard standard isotherm [21]. The total pore volume V_{total} was determined from the amount of nitrogen adsorbed at nitrogen relative pressure $p/p_0 = 0.99$.

Temperature-programmed reduction (TPR) measurements of the catalysts (0.025 g) were performed with a H_2/N_2 mixture (10 mol% H_2), flow rate 50 mL min^{-1} and linear temperature increase 20 °C min^{-1} up to 1 000 °C. A change in H_2 concentration was detected with a mass spectrometer Omnistar 300 (Pfeiffer Vacuum). Reduction of the grained CuO (0.16–0.32 mm) was performed in each experiment to calculate absolute values of hydrogen consumed during reduction.

Temperature-programmed desorption (TPD) of NH_3 and CO_2 was carried out to examine acid and basic properties of the catalysts surface. The measurements were accomplished with 0.1 g of a catalyst in the temperature range 20–1000 °C using flow rate 20 mL min^{-1}, helium as a carrier gas and NH_3 or CO_2 as an adsorbing gas. Prior to the measurement, each sample was calcined in helium at 500 °C, then cooled to 30 °C and an excess of NH_3 or CO_2 (ten doses, 840 μL each) was applied on the sample. Then, the sample was flushed with helium for 1 h to remove physically adsorbed NH_3 or CO_2 and after that heating rate of 20 °C min^{-1} was applied. A change in NH_3 or CO_2 concentration was detected with a mass spectrometer Omnistar 300 (Pfeiffer Vacuum). During the experi-

ments the following mass contributions m/z were collected: 2-H_2, 16-NH_3, 18-H_2O, 28-N_2, 32-O_2, 44-N_2O/CO_2, and 46-NO_2.

2.3. Catalytic experiments

Catalytic reaction was carried out in a glass reactor in the temperature range from 50 to 300 °C (the furnace temperature was linearly increased with the rate of 2 °C min^{-1}). The monolithic catalyst was examined at 20 m^3 kg^{-1} h^{-1} space velocity without any pretreatment. Temperature was measured inside the reactor before and after the monolith and the average temperature was taken as catalyst temperature. The inlet concentration of ethanol in the air was 0.8 g/m^3. Before the experiment the catalyst was kept under the feed stream until the outlet concentration became constant. Reaction mixture was analyzed by a gas chromatograph Hewlett-Packard 6890 and concentrations of CO and CO_2 were monitored using a Siemens Ultramat 23 infrared analyzer. Conversion C and selectivity to carbon dioxide S were calculated as given elsewhere [15]. Temperature T_{50} (the temperature at which 50% conversion was observed) was employed as a measure of catalyst performance. The catalytic activity of gold catalysts was also assessed in terms of turn-over frequency (TOF). The TOF was calculated in moles of converted ethanol per mol of surface gold atoms employing the average Au particle size determined by electron microscopy. The TOF was evaluated at 60 °C, the ethanol conversion was 5.1% for the AuCeZr catalyst (space velocity 20 m^3 kg^{-1} h^{-1}) and 12.5% for the Au/CeZr catalyst (space velocity 75 m^3 kg^{-1} h^{-1}). The apparent activation energy was calculated for ethanol conversions lower than 30% using the Arrhenius plot ln(ln(1-C)/-1) = f(1/T). Reaction by-products were identified using GC–MS analysis and the catalyst selectivity was evaluated as the selectivity to CO_2 at 95% and 99% conversion (S_{95} and S_{99}, respectively).

3. Results

The Au content in the prepared catalysts determined by ICP-AES analysis was 1.56 wt.% Au for the AuCeZr catalyst and 1.76 wt.% Au for the Au/CeZr catalyst.

X-ray powder diffractograms of parent ceria-zirconia mixed oxide and both types of gold catalysts are shown in Fig. 1. The XRD data are consistent with that reported for $Ce_xZr_{1-x}O_2$ solid solutions [22]. The well-known ceria-zirconia phase diagram indicates that with the addition of zirconia, cubic ceria is progressively transformed into t″, t″, t, m phase with metastable pyrochlore-like structures. In comparison with pure CeO_2 (diffractions at 28.7°, 33.3°, 47.8° and 56.8°), the diffraction lines in Fig. 1 are shifted to higher angles (29.2°, 33.8°, 48.6°, and 57.8°) due to the incorporation of Zr. The position of the (111) diffraction line of the cubic phase at 29.2° corresponds to the composition of the ceria-zirconia solid solution $Ce_{0.5}Zr_{0.5}O_2$ [22]. For the homogeneous $Ce_{0.5}Zr_{0.5}O_2$ the structure is t″, i.e. cubic for the cation position but the oxygens are displaced from their regular position. However, the splitting of diffraction lines at higher angles (Fig. 1) points to the presence of at least two solid solutions with slightly different cell constants [23]. The mean size of ceria-zirconia crystallites was not influenced by the addition of gold and was 11 nm for parent ceria-zirconia and both gold catalysts. The mean size of Au crystallites determined using Scherrer equation was 23 nm for the AuCeZr catalyst. In the case of the Au/CeZr catalyst, the gold crystallites were not detected.

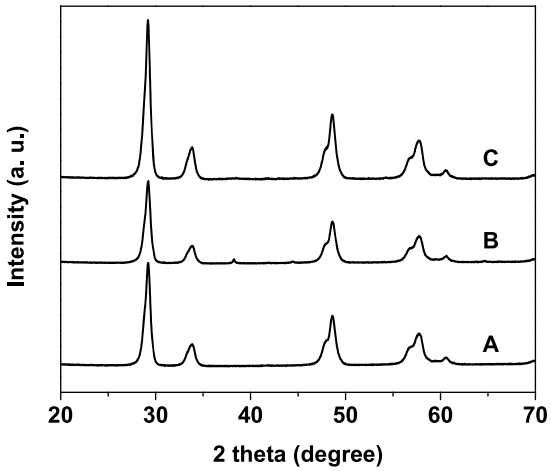

Fig. 1. X-ray diffraction patterns of CeZr (A), AuCeZr (B) and Au/CeZr (C) catalysts.

Adsorption of nitrogen at −196 °C showed that the adsorption isotherms of the support and catalysts are similar and correspond to the combination of I and IV type isotherms according to IUPAC classification [24], which is typical for samples containing both micropores and mesopores. From Table 1 it is seen that after the deposition of gold surface area of the catalysts decreased (from 56 m^2/g to 36–38 m^2/g), which is in line with earlier studies [20].

AuCeZr and Au/CeZr catalysts were studied by STEM to measure the size distribution of Au nanoparticles and observe their dispersion on ceria-zirconia support. Loading of Au nanoparticles in both catalysts is so low that selected-area electron diffraction (SAED) did not reveal their presence. In the TEM mode, the detection is complicated mainly by diffraction contrast. This is illustrated in Fig. 2A and B, where Au nanoparticles can be only hardly discerned. Therefore, the HRTEM images were acquired (Fig. 2C, D) to distinguish Au nanoparticles from $Ce_{0.5}Zr_{0.5}O_2$ by the spacing of lattice fringes. Moreover, Fig. 3 shows the STEM results, where contrast depends on the atomic number by the factor of 3/2 (Zr = 40, Ce = 58, Au = 79). Here, the particles can be clearly discerned. In addition, every particle counted in the particle analysis was checked by EDX spectroscopy. The particle size distribution histograms were plotted based on measurements of 100 Au particles in each sample. Maximum length of particles was measured as well as the corresponding perpendicular length. As the particles are mostly isometric (similar results of size distribution were obtained for both catalysts), the geometric average corresponding to the diameter of a circle with same area is shown in Fig. 3 together with HAADF images illustrating the dispersion of Au nanoparticles. Both samples display lognormal size distribution. The AuCeZr catalyst contains Au nanoparticles of an average size of 13.2 nm with a wide size distribution (from 3.4 to 34.8 nm) while the Au particles from the Au/CeZr catalyst display a narrow size distribution (from 2.1 to 11.6 nm, with the exception of one particle with the diameter of 17.3 nm) and the average size of 6.7 nm. Moreover, the Au particles

Table 1
Physicochemical properties of investigated catalysts.

Catalyst	S_{meso} (m^2 g^{-1})	S_{BET} (m^2 g^{-1})	V_{total} (cm$^3_{liq}$ g^{-1})	H_2-TPR[a] (mmol g^{-1})	NH_3-TPD[a] (mmol g^{-1})	CO_2-TPD[a] (mmol g^{-1})	Ce 3d$_{5/2}$ (V) (eV)	Au 4f$_{7/2}$ (eV)
CeZr	37	56	0.227	0.88	0.06	0.12	885.4 (29%) Ce^{3+}902.1 (71%) Ce^{4+}	–
AuCeZr	24	38	0.164	0.85	0.08	0.08	885.4 (25%) Ce^{3+}902.1 (75%) Ce^{4+}	84.2
Au/CeZr	28	36	0.195	1.02	0.11	0.10	885.4 (27%) Ce^{3+}902.1 (73%) Ce^{4+}	84.3

[a] corresponding to total peak area between 25 and 900 °C.

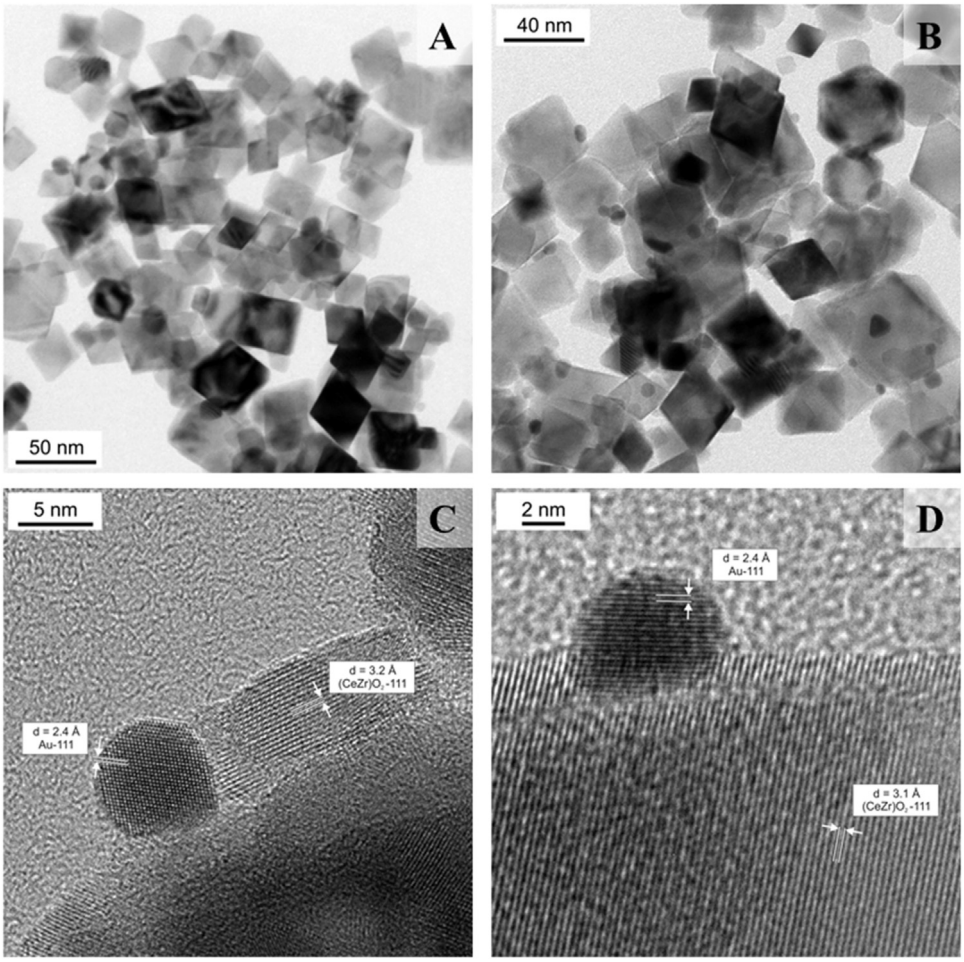

Fig. 2. Electron microscopy images of AuCeZr (A, C) and Au/CeZr (B, D) catalysts.

are evenly dispersed in both samples with a higher concentration of particles in the Au/CeZr catalyst.

The reducibility of the catalysts was examined by temperature-programmed reduction using hydrogen as a reducing agent (Fig. 4). The pristine ceria-zirconia showed two peaks centred at 353 °C and 513 °C that can be ascribed to the reduction of surface cerium and bulk cerium, respectively. In the case of the AuCeZr catalyst, both low-temperature and high-temperature reduction peak of cerium are shifted to lower temperatures (213 °C and 273 °C, respectively). This shows that the reduction of Ce^{4+} was promoted by gold nanoparticles. Even larger shift of the two reduction peaks to lower temperatures can be seen with the Au/CeZr catalyst, exhibiting a main reduction peak at 161 °C with a shoulder at 91 °C. This catalyst was practically reduced in a single step, which points to a high mobility of the lattice oxygen ions [25]. The extent of the reduction was larger for the Au/CeZr catalyst with a H_2 uptake of 1.02 mmol/g, while the AuCeZr and CeZr catalysts exhibited similar values (0.85 and 0.88 mmol/g, respectively, Table 1). This shows a marked effect of preparation method on the reducibility of ceria-zirconia support, which is connected with Au particle size, as evidenced by electron microscopy (Fig. 3). The reduction of the support surface strongly anchored with finely dispersed Au particles occurs at lower temperature and the reduction of the support being in contact with larger gold agglomerates and/or unaffected by Au, occurs at higher temperature [20].

The surface composition of the catalysts was analyzed by XPS. The results are summarized in Table 1. The catalysts exhibited amount of Ce^{3+} between 25 and 29%. It is seen that the modification of ceria-zirconia with gold did not change the characteristics of the support. AuCeZr and Au/CeZr catalysts exhibited similar binding energy of Au $4f_{7/2}$ (84.2 and 84.3 eV, respectively), which corresponds to metallic gold [26]. In both cases, the Au $4f_{7/2}$ peak possessed additional shoulders at 85.3 and 85.4 eV, respectively. Quantitative fits led to a composition of about 88% metallic and 12% of partially oxidized Au species for the AuCeZr catalyst; 73% metallic and 27% of partially oxidized Au species was observed in the Au/CeZr catalyst. The atomic concentration of Au was 2.0% in the AuCeZr catalyst and 3.2% in the Au/CeZr catalyst.

The acidity of investigated catalysts was studied using temperature-programmed desorption of ammonia (NH_3-TPD). The desorption features from CeZr, AuCeZr and Au/CeZr catalyst are shown in Fig. 5. Desorption of ammonia proceeded mainly in the temperature range from 25 to 300 °C. It shows that the catalysts possess only weak acid sites. The surface species responsible for this acidity are coordinatively unsaturated Ce^{4+} and Zr^{4+} ions, which possess an uncompensated positive charge and create Lewis acidity [25]. For all catalysts, a distinct desorption peak can be recognized at 102 °C with a shoulder at ~184 °C. Thus, both gold catalysts as well as pure ceria-zirconia exhibited similar strength of acid sites. The amount of acid sites corresponding to total peak area between 25 and 900 °C in the NH_3-TPD profiles is shown in Table 1. Ammonia adsorbs on the surface of the catalysts, therefore it may be more correct to compare the amount of acid sites taking into account the different surface area of the catalysts S_{BET}. The acid site density (amount of NH_3 adsorbed per m^2 of catalyst surface)

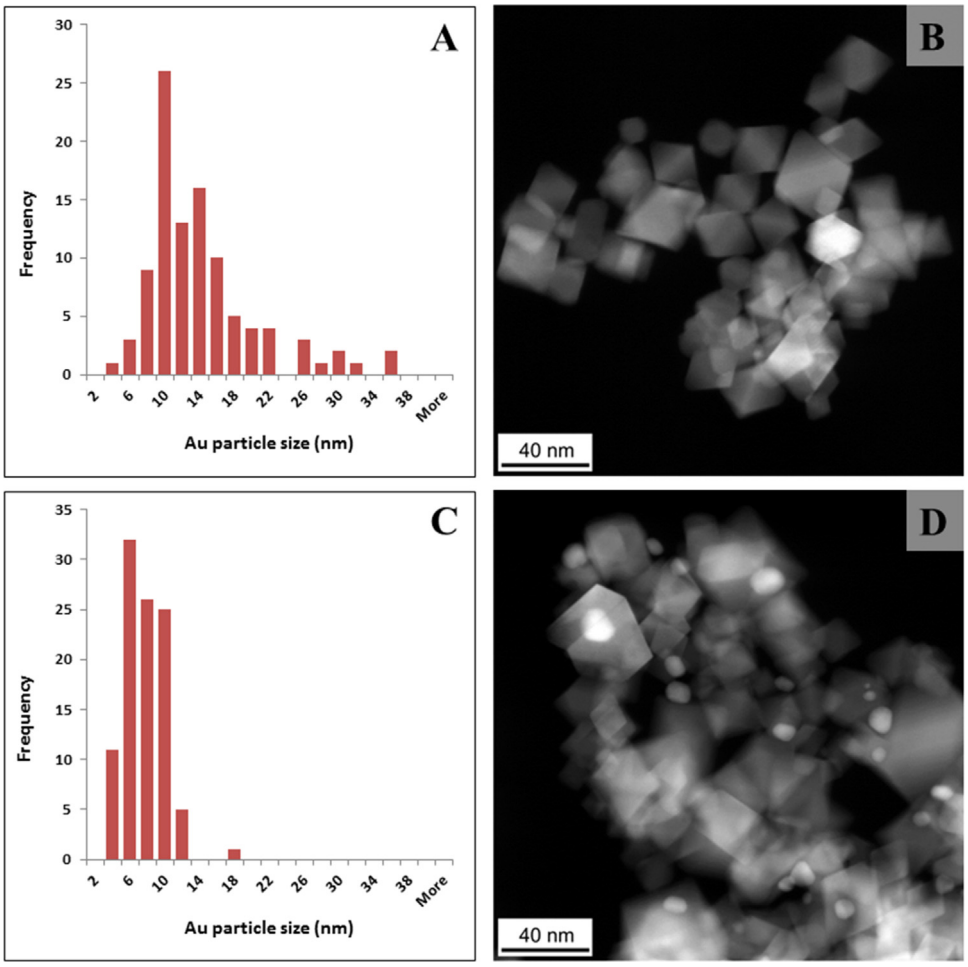

Fig. 3. Au particle size distribution and HAADF images of AuCeZr (A, B) and Au/CeZr (C, D) catalysts.

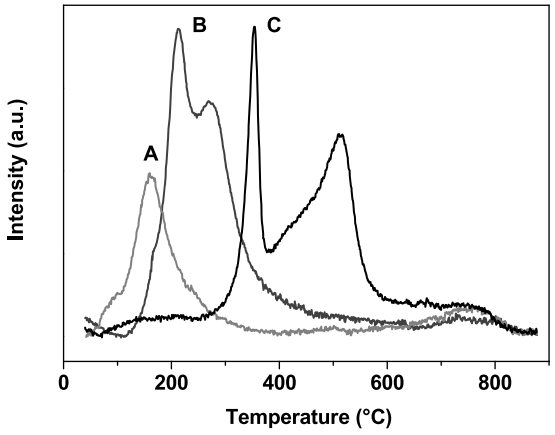

Fig. 4. H_2-TPR profiles of Au/CeZr (A), AuCeZr (B) and CeZr (C) catalysts.

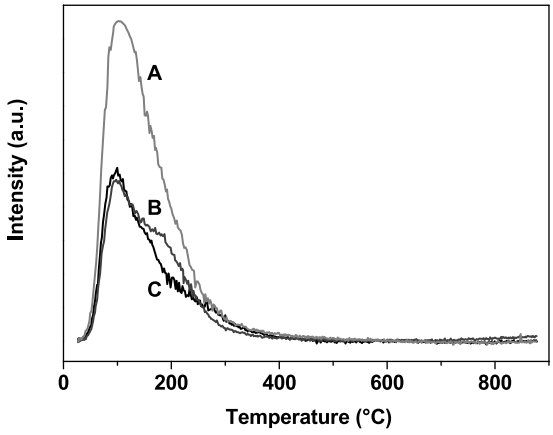

Fig. 5. NH_3-TPD profiles of Au/CeZr (A), AuCeZr (B) and CeZr (C) catalysts.

increased in the order CeZr < AuCeZr < Au/CeZr (0.0010 mmol/m^2, 0.0020 mmol/m^2 and 0.0029 mmol/m^2, respectively).

The basicity of the catalysts was characterized by temperature-programmed desorption of carbon dioxide (CO_2-TPD). The patterns of CO_2 desorption from CeZr, AuCeZr and Au/CeZr catalyst are shown in Fig. 6. The CeZr and Au/CeZr catalysts exhibited a desorption peak at 110 °C. With the AuCeZr catalyst, a small shift of the main desorption peak to 126 °C was revealed. Nevertheless, all studied catalysts possessed only basic sites of low strength. The amount of basic sited corresponding to total peak area between 25 and 900 °C in the CO_2-TPD profiles is shown in Table 1. The density of basic sites (amount of CO_2 adsorbed per m^2 of catalyst surface) increased in the order CeZr ~ AuCeZr < Au/CeZr (0.0022 mmol/m^2, 0.0020 mmol/m^2 and 0.0029 mmol/m^2, respectively).

The catalytic performance of the catalysts in the total oxidation of ethanol is summarized in Table 2. In the case of monoliths washcoated with ceria-zirconia mixed oxide, the temperature of 50% conversion (T_{50}) determined by light-off experiments decreased linearly with increasing washcoat loading up to ~15 wt.%. The catalysts with washcoat loading 19.5 and 21.5 wt.% exhibited the same

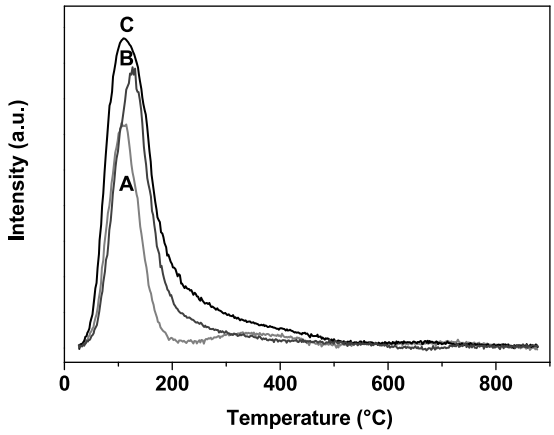

Fig. 6. CO_2-TPD profiles of Au/CeZr (A), AuCeZr (B) and CeZr (C) catalysts.

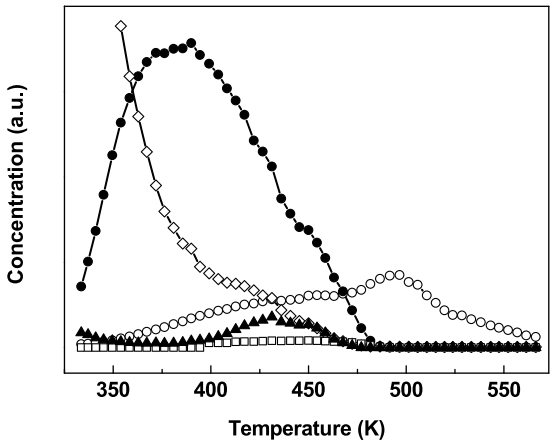

Fig. 7. Evolution of by-products during ethanol oxidation over the Au/CeZr catalyst: ◊ ethanol, ○ ethylene, ● acetaldehyde, □ acetic acid, ▲ ethyl acetate.

Table 2
Performance of catalysts in ethanol oxidation (0.8 g/m^3 in air, space velocity 20 m^3 kg^{-1} h^{-1}, temperature ramp 2 °C min^{-1}).

Catalyst	Washcoat (wt.%)	T_{50}(°C)	T_{90}(°C)	S_{95}(%)	S_{99}(%)
CeZr	4.1	274	303	84	97
CeZr	8.8	256	281	86	97
CeZr	13.3	240	271	88	98
CeZr	19.5	233	267	90	98
CeZr	21.9	233	262	95	98
AuCeZr	5.5	142	210	35	57
AuCeZr	9.2	129	196	18	55
AuCeZr	14.7	112	198	54	71
AuCeZr	16.5	113	204	59	74
AuCeZr	20.0	120	201	55	71
Au/CeZr	20.9	80	133	44	76
Au/CeZr	21.1	74	125	47	73

T_{50} (233 °C). Selectivity to CO_2 can be even more important than the catalytic performance due to the fact that some by-products formed during the oxidation may be more detrimental to the environment than the initial compounds. For example, acetaldehyde and/or acetic acid can be formed during ethanol oxidation [27]. It is known that over noble metal catalysts, ethanol oxidation may follow two parallel reaction paths – direct oxidation to CO_2, and partial oxidation to acetaldehyde, which is then oxidized to CO_2 [28]. In ethanol oxidation over CeZr catalysts, acetaldehyde and acetic acid were observed as main by-products, together with traces of ethylene and carbon monoxide. The selectivity to CO_2 at 95% conversion increased with increasing washcoat loading (from 84 to 95%). At 99% conversion, the selectivity to carbon dioxide was 97–98% (Table 2).

With the AuCeZr catalysts (monoliths washcoated with gold/ceria-zirconia powder), the catalytic performance increased linearly with increasing washcoat loading up to ~15 wt.%. For the AuCeZr catalyst with 20 wt.% washcoat loading, the T_{50} was 120 °C, i.e. 113 °C less than for its CeZr analogue. However, the selectivity to CO_2 was much lower due to the formation of various by-products. Acetaldehyde and ethylene were detected as main by-products, together with small amounts of acetic acid and ethyl acetate and traces of carbon monoxide. Nevertheless, it should be noted that the selectivity reported in Table 2 was determined using light-off experiments and that at prolonged reaction times much higher selectivity to CO_2 can be achieved (89–100%).

The Au/CeZr catalysts prepared by depositing of gold on the monolith already washcoated with ceria-zirconia exhibited better catalytic performance than the catalysts prepared using gold/ceria-zirconia powder (Table 2). In comparison with AuCeZr catalysts, the T_{50} was by 40 °C lower. Similar results were reported by Santos et al. [29], who showed that the light-off curve of ethanol oxidation over Au/TiO_2 catalysts with gold particle size 4.0 nm was significantly shifted to lower temperatures in comparison with that for 9.1 nm. In terms of turn-over frequency, the Au/CeZr catalyst with ~20 wt.% washcoat loading would be approximately four times more active than its AuCeZr analogue (the TOF was 1.3×10^{-2} s^{-1} and 3.2×10^{-3} s^{-1}, respectively). However, it should be noted that the TOF was computed in moles of converted ethanol per mol of surface gold atoms, i.e. the contribution to the activity from the bare support was neglected; moreover, not all surface Au atoms but only perimeter of Au particles may be active in the reaction [30,31]. Finally, the selectivity of the Au/CeZr catalysts to CO_2 was comparable with the AuCeZr catalysts and the same by-products were observed, with the exception of carbon monoxide. The detailed distribution of by-products is shown in Fig. 7.

4. Discussion

The AuCeZr and Au/CeZr catalysts were prepared by the direct anionic exchange method of gold species with hydroxyl groups of the support. The nominal Au loading and Au concentration in the impregnation solution were the same for both types of the catalysts. Thus, the different Au particle size distribution (larger Au particles observed in the AuCeZr catalyst) might be connected with some other detail of catalysts preparation. In order to elucidate the possible effect of nitric acid solution that was used during the preparation of the AuCeZr catalysts, the following experiment was done. The Au/CeZr catalyst was washed for 2 h with diluted nitric acid solution (1.4 wt.%) under dynamic conditions, dried at 120 °C overnight and calcined at 300 °C for 4 h. After that a catalytic test was made. The difference between the standard Au/CeZr catalyst and that subjected to washing with acid solution was in the frame of the experimental error (the T_{50} was by 4 °C lower). Therefore, it can be concluded that the use of diluted nitric acid solution during the catalysts preparation was not the factor which resulted in different properties of the AuCeZr catalysts. Another aspect of the preparation procedure that might influence Au particle size distribution can be the mass transport resistance of the washcoat layer. For the preparation of the powder AuCeZr catalyst, a very fine ceria-zirconia powder was used (particle size < 50 nm by BET). Therefore, a high fraction of the support's surface was immediately accessible for the anionic exchange with gold anions from the impregnation solution. On the other hand, when a monolith already washcoated with ceria-zirconia was immersed into the impregnation solution, it can be expected that initially only a superficial layer of the ceria-zirconia washcoat would be readily accessible for the

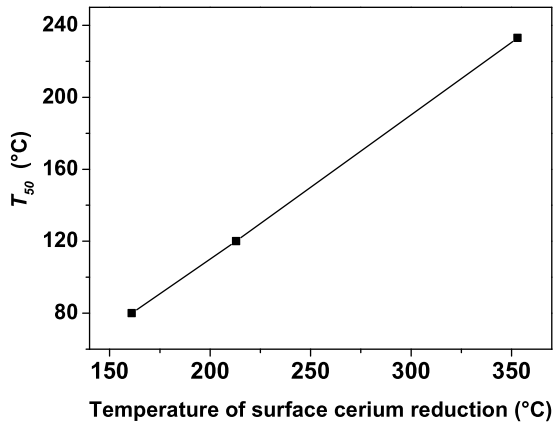

Fig. 8. Correlation between T_{50} in ethanol oxidation and temperature of surface cerium reduction in H_2-TPR experiments for the Au/CeZr, AuCeZr and CeZr catalysts.

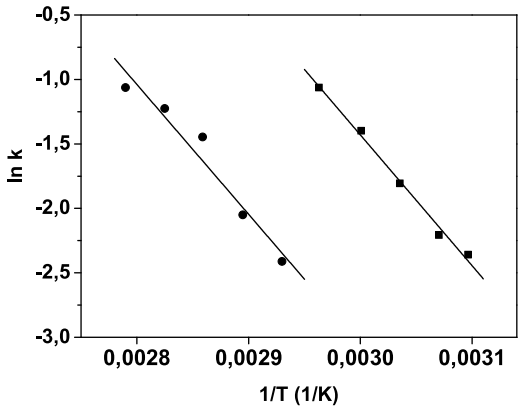

Fig. 9. Arrhenius plot for ethanol oxidation over AuCeZr (●) and Au/CeZr (■) catalysts.

anionic exchange with gold anions, while the exchange in the bulk of the washcoat would be hindered by mass transport resistances.

By H_2-TPR measurements (Fig. 4) it was shown that the addition of Au to ceria-zirconia significantly promoted the reduction of surface cerium. Moreover, there was a considerable difference between H_2-TPR profiles of AuCeZr and Au/CeZr catalysts. The H_2-TPR peaks of Au/CeZr catalyst are shifted to lower temperatures in comparison with the AuCeZr catalysts (Fig. 4). Thus, there is a good correlation between H_2-TPR profiles and catalytic performance of investigated catalysts (Fig. 8). The temperature of the main reduction peak of the catalysts increased in the order Au/CeZr > AuCeZr > CeZr (161, 213 and 353 °C, respectively). At the same time, the catalytic performance in ethanol oxidation decreased in the same order (the T_{50} was 80, 120 and 233 °C, respectively). A similar correlation between reducibility and catalytic performance was observed for ethanol oxidation over $Pt/Ce_{0.5}Zr_{0.5}O_2$ catalysts [32].

It was demonstrated earlier that the catalytic performance in alcohol oxidation can be influenced by noble metal loading and/or particle size [33–35]. Minicò et al. [36] concluded that the high activity of Au/Fe_2O_3 catalyst in ethanol oxidation was related to the capacity of highly dispersed gold to weaken the Fe–O bond thus increasing the mobility of the lattice oxygen which is involved in ethanol oxidation probably through a Mars–van Krevelen reaction mechanism. Similarly, Solsona et al. [37,38] attributed the improved catalytic performance of the Au/Co_3O_4 catalysts in ethanol oxidation to the enhancement of the redox properties of the support oxide induced by gold due to the introduction of surface defects at the gold/oxide interface, involved in VOC activation. Recently, Holz et al. [39] proposed two types of active sites for ethanol oxidation over Au/TiO_2: (i) the perimeter of Au nanoparticles, and (ii) the support. They reported that the presence of highly dispersed Au nanoparticles induced a new oxidation pathway. The second type of active sites located on the support was likely to follow the Mars–van Krevelen mechanism. The presence of Au nanoparticles also increased the activity of the support due to its enhanced reducibility. Similarly to the Au/TiO_2 catalysts, Mars–van Krevelen mechanism implying lattice oxide ions as the active oxygen species together with oxygen activation on the perimeter of Au nanoparticles is likely to apply also to the ethanol oxidation over the investigated $Au/Ce_{0.5}Zr_{0.5}O_2$ catalysts. A more detailed study is needed to deconvolute the contribution to the catalytic performance from Au particles and from the support.

If we consider the average size of Au nanoparticles in the present $Au/Ce_{0.5}Zr_{0.5}O_2$ catalysts, hemispherical shape of the particles and actual Au loading, the Au/CeZr catalyst would contain 8.6 times more Au particles than the AuCeZr catalyst, and the total perimeter of all nanoparticles in the Au/CeZr catalyst would be 4.4 times larger than in the AuCeZr catalyst. Consequently, a higher number of active sites would be available on the perimeter of Au nanoparticles and the metal-support interaction would be more pronounced, which is in line with obtained H_2-TPR and catalytic results. The Au/CeZr catalyst with average Au particle size of 6.7 nm exhibited lower temperature of surface cerium reduction (161 °C) than the AuCeZr catalyst with average size of Au nanoparticles 13.2 nm (213 °C). Dobrosz-Gómez et al. [20] reported earlier that the reduction of the support surface strongly anchored with finely dispersed Au particles occurs at lower temperature than the reduction of the support being in contact with larger gold agglomerates. Moreover, the H_2-TPR experiments suggest that the Au/CeZr catalyst not only has a lower reduction temperature but also appeared to have improved oxygen storage capacity (evidenced by the higher H_2 consumption). While the AuCeZr and CeZr catalysts exhibited similar values of hydrogen consumption (0.85 and 0.88 mmol/g, respectively, Table 1), the Au/CeZr catalyst reached 1.02 mmol/g. It is known that the improved oxygen storage capacity may contribute to higher catalytic performance of the catalysts. However, from Fig. 8 it is seen that the catalytic performance correlated with reducibility of the catalysts, while the effect of higher oxygen storage capacity of the Au/CeZr catalyst in comparison with the other catalysts was not pronounced. Concluding, the examples of CeZr and AuCeZr catalysts showed that the enhanced redox properties appear to promote the oxidation rates significantly. Therefore, it can be assumed that the significantly higher catalytic activity observed for the Au/CeZr catalysts is mainly connected with the further enhanced surface redox properties of these catalysts. In order to disclose the possible difference in the nature of active sites, the Arrhenius plot was constructed for the AuCeZr and Au/CeZr catalysts with ~20 wt.% washcoat loading (Fig. 9). However, the apparent activation energy was the same for both types of the catalysts (84 kJ/mol). This points to the same nature of the active sites in both AuCeZr and Au/CeZr catalysts. Therefore, the increased catalytic activity of the Au/CeZr catalyst may be ascribed to improved redox properties due to the presence of highly dispersed Au nanoparticles, which possess a higher number of active sites as discussed above.

It was shown earlier that acid-base properties of VOC oxidation catalysts represent an important parameter for their catalytic performance. The changes in acidity and basicity of the catalyst surface can influence adsorption-desorption equilibria of reactants and/or reaction mechanism [40]. Recently, it was proposed that the Lewis acidity of the metal center is a key factor influencing the performance of some types of catalysts in ethanol oxidation [41]. On the other hand, the acid sites usually decrease the selectivity to CO_2

due to the formation of by-products (mainly acetaldehyde) and a decreased acidity thus may lead to improved selectivity [42]. In our case, all studied catalysts exhibit the same strength of acid sites. The density of acid sites increased in the order CeZr < AuCeZr < Au/CeZr (0.0010 mmol/m^2, 0.0020 mmol/m^2 and 0.0029 mmol/m^2, respectively). The increased amount of acid sites after gold introduction can be attributed to coordinatively unsaturated Ce^{4+} and Zr^{4+} ions, which are in contact with gold nanoparticles. On the other hand, the AuCeZr and Au/CeZr catalysts exhibited similar selectivity to CO_2 (S_{99} was 71–76%), while the CeZr catalyst was much more selective (S_{99} = 98%). Thus, the differences in selectivity among the studied catalysts can be tentatively ascribed to different reaction mechanism over gold catalysts in comparison with pure $Ce_{0.5}Zr_{0.5}O_2$, while the effect of catalyst acidity would be negligible. Concerning the basicity of the catalysts, it was reported that increased basicity can positively influence the activity of the catalyst due to strong adsorption of the oxidized alcohol [40]. In the present case, all studied catalysts exhibited similar strength of basic sites. The density of basic sites increased in the order CeZr ~ AuCeZr < Au/CeZr (0.0022 mmol/m^2, 0.0020 mmol/m^2 and 0.0029 mmol/m^2, respectively), while the catalytic performance increased in the order CeZr < AuCeZr < Au/CeZr (the T_{50} was 233, 120 and 80 °C, respectively). However, taking into account the different nature of the studied catalysts (the presence vs. the absence of gold, the different Au particle size in the case of gold catalysts), the possible effect of amount of basic sites on catalytic activity cannot be judged.

5. Conclusions

Cordierite monolithic catalysts with gold nanoparticles supported on $Ce_{0.5}Zr_{0.5}O_2$ were prepared either by washcoating with powder gold/ceria-zirconia (catalyst AuCeZr) or by depositing of gold on the monolith washcoated with ceria-zirconia (catalyst Au/CeZr). The AuCeZr catalyst possessed wide Au particle size distribution centred at 13.2 nm, while the Au/CeZr catalyst exhibited narrow Au particle size distribution centred at 6.7 nm. The gold catalysts were compared with pure $Ce_{0.5}Zr_{0.5}O_2$. In gas-phase oxidation of ethanol, the monolith washcoated only with ceria-zirconia converted 50% of ethanol at 233 °C. The AuCeZr catalyst reached the same conversion at 120 °C and the Au/CeZr catalyst at 80 °C. A good correlation was observed between H_2-TPR profiles and catalytic performance of the catalysts. The superior catalytic performance of the Au/CeZr catalyst was ascribed to the presence of highly dispersed Au nanoparticles, which enhanced the reducibility of the catalyst.

Acknowledgements

The financial support of the Grant Agency of the Czech Republic (project No. 13-24186P) is gratefully acknowledged. The authors thank Dr. P. Dytrych and M. Koštejn for XPS analysis and Dr. K. Jirátová for TPR and TPD measurements. M. K. would like to acknowledge the financial support from the CENTEM project, Reg. No. CZ.1.05/2.1.00/03.0088, cofunded by the ERDF as part of the Ministry of Education, Youth and Sports OP RDI programme and, in the follow-up sustainability stage, supported through CENTEM PLUS (LO1402) by financial means from the Ministry of Education, Youth and Sports under the National Sustainability Programme I.

References

[1] R.G. Derwent, M.E. Jenkin, S.M. Saunders, M.J. Pilling, P.G. Simmonds, N.R. Passant, G.J. Dollard, P. Dumitrean, A. Kent, Atmos. Environ. 37 (2003) 1983–1991.
[2] M.M. Galloway, P.S. Chhabra, A.W.H. Chan, J.D. Surratt, R.C. Flagan, J.H. Seinfeld, F.N. Keutsch, Atmos. Chem. Phys. 9 (2009) 3331–3345.
[3] F.I. Khan, A.K. Ghoshal, J. Loss Prev. Process Ind. 13 (2000) 527–545.
[4] A.C. Gluhoi, B.E. Nieuwenhuys, Catal. Today 119 (2007) 305–310.
[5] P.O. Larsson, A. Andersson, Appl. Catal. B 24 (2000) 175–192.
[6] J.J. Spivey, Ind. Eng. Chem. Res. 26 (1987) 2165–2180.
[7] M. Haruta, T. Kobayashi, H. Sano, N. Yamada, Chem. Lett. 16 (1987) 405–408.
[8] S. Scirè, L.F. Liotta, Appl. Catal. B 125 (2012) 222–246.
[9] S. Scirè, S. Minicò, C. Crisafulli, C. Satriano, A. Pistone, Appl. Catal. B 40 (2003) 43–49.
[10] Q. Fu, A. Weber, M. Flytzani-Stephanopoulos, Catal. Lett. 77 (2001) 87–95.
[11] S. Minicò, S. Sciré, C. Crisafulli, R. Maggiore, S. Galvagno, Appl. Catal. B 28 (2000) 245–251.
[12] J.I. Gutiérrez-Ortiz, B. de Rivas, R. López-Fonseca, J.R. González-Velasco, Appl. Catal. A 269 (2004) 147–155.
[13] J.I. Gutierrez-Ortiz, B. de Rivas, R. Lopez-Fonseca, J.R. Gonzalez-Velasco, Appl. Catal. B 65 (2006) 191–200.
[14] M. Boaro, C. de Leitenburg, G. Dolcetti, A. Trovarelli, J. Catal. 193 (2000) 338–347.
[15] J. Gaálová, P. Topka, L. Kaluža, O. Šolcová, Catal. Today 175 (2011) 231–237.
[16] L. Matějová, P. Topka, L. Kaluža, S. Pitkäaho, S. Ojala, J. Gaálová, R.L. Keiski, Appl. Catal. B 142 (2013) 54–64.
[17] P. Topka, R. Delaigle, L. Kaluža, E.M. Gaigneaux, Catal. Today 253 (2015) 172–177.
[18] L.M. Martínez Tejada, M.I. Domínguez, O. Sanz, M.A. Centeno, J.A. Odriozola, Gold Bull. 46 (2013) 221–231.
[19] L.F. Liotta, A. Longo, G. Pantaleo, G. Di Carlo, A. Martorana, S. Cimino, G. Russo, G. Deganello, Appl. Catal. B 90 (2009) 470–477.
[20] I. Dobrosz-Gómez, I. Kocemba, J.M. Rynkowski, Appl. Catal. B 88 (2009) 83–97.
[21] A. Lecloux, J.P. Pirard, J. Colloid Interface Sci. 70 (1979) 265–281.
[22] L. Lan, S. Chen, Y. Cao, M. Zhao, M. Gong, Y. Chen, J. Colloid Interface Sci. 450 (2015) 404–416.
[23] L.F. Liotta, A. Macaluso, A. Longo, G. Pantaleo, A. Martorana, G. Deganello, Appl. Catal. A 240 (2003) 295–307.
[24] S.J. Gregg, K.S.W. Sing, Adsorption, Surface Area and Porosity, Academic Press New York, 1982.
[25] B. de Rivas, R. López-Fonseca, M.A. Gutiérrez-Ortiz, J.I. Gutiérrez-Ortiz, Appl. Catal. B 104 (2011) 373–381.
[26] R. Leppelt, B. Schumacher, V. Plzak, M. Kinne, R.J. Behm, J. Catal. 244 (2006) 137–152.
[27] G. Avgouropoulos, E. Oikonomopoulos, D. Kanistras, T. Ioannides, Appl. Catal. B 65 (2006) 62–69.
[28] A.A. Barresi, G. Baldi, Chem. Eng. Comm. 123 (1993) 31–42.
[29] V.P. Santos, S.A.C. Carabineiro, P.B. Tavares, M.F.R. Pereira, J.J.M. Órfão, J.L. Figueiredo, Appl. Catal. B 99 (2010) 198–205.
[30] L.M. Petkovic, S.N. Rashkeev, D.M. Ginosar, Catal. Today 147 (2009) 107–114.
[31] M.S. Avila, C.I. Vignatti, C.R. Apesteguía, T.F. Garetto, Chem. Eng. J. 241 (2014) 52–59.
[32] P. Topka, L. Kaluža, J. Gaálová, Chem. Pap. 70 (2016) 898–906.
[33] K. Soukup, D. Petráš, P. Topka, P. Slobodian, O. Šolcová, Catal. Today 193 (2012) 165–171.
[34] K. Soukup, P. Topka, V. Hejtmánek, D. Petráš, V. Valeš, O. Šolcová, Catal. Today 236 (2014) 3–11.
[35] L. Matějová, P. Topka, K. Jirátová, O. Šolcová, Appl. Catal. A 443 (2012) 40–49.
[36] S. Minicò, S. Scirè, C. Crisafulli, R. Maggiore, S. Galvagno, Appl. Catal. B 28 (2000) 245–251.
[37] B.E. Solsona, T. Garcia, C. Jones, S.H. Taylor, A.F. Carley, G.J. Hutchings, Appl. Catal. A 312 (2006) 67–76.
[38] B. Solsona, E. Aylón, R. Murillo, A.M. Mastral, A. Monzonís, S. Agouram, T.E. Davies, S.H. Taylor, T. Garcia, J. Hazard. Mater. 187 (2011) 544–552.
[39] M.C. Holz, K. Tolle, M. Muhler, Catal. Sci. Technol. 4 (2014) 3495–3504.
[40] R. Beauchet, P. Magnoux, J. Mijoin, Catal. Today 124 (2007) 118–123.
[41] P. Gonzalez-Navarrete, M. Schlangen, X.N. Wu, H. Schwarz, Chem. Eur. J. 22 (2016) 3077–3083.
[42] J. Ludvíková, K. Jirátová, J. Klempa, V. Boehmová, L. Obalová, Catal. Today 179 (2012) 164–169.